Synthesis and Characterization of Mechanically Alloyed $Al/Al_xMg_{1-x}B_2$ Composites

O. Marcelo Suárez[1*], José Vázquez[2], Luvina Reyes-Russi[3],

[1] *Engineering Science and Materials Department, University of Puerto Rico-Mayagüez*
P.O. Box 9044, Mayagüez 00681-9044, Puerto Rico
[2] *Material Processes & Producibility, Raytheon Missile Systems, Arizona USA*
[3] *WorleyParsons, Arcadia Ltd., California, USA*

ABSTRACT

The use of high energy ball milling (HEBM) was investigated as an alternative method to synthesize aluminum matrix composites reinforced with $Al_xMg_{1-x}B_2$ particles. HEBM allowed achieving appropriate mixing and wettability between the composite components. After a 900°C treatment under vacuum, the resulting material had a mixed microstructure of dispersoids and submicron $Al_xMg_{1-x}B_2$ (hereon also referred as $(AlMg)B_2$) particles embedded in the Al matrix containing also β (Al_3Mg_2) + Al eutectic. After processing the size distribution of $Al_xMg_{1-x}B_2$ particles included large particles (<23μm) and submicron ones. Vickers microhardness measured on the composite matrix revealed that the highest matrix hardness was obtained in samples containing 5 wt.% $Al_xMg_{1-x}B_2$ where larger amounts of nanosized reinforcement particles were present. X-ray diffraction studies showed the formation of $Al_xMg_{1-x}B_2$ in the mechanically alloyed composites. In summary, the results buttressed the feasibility of fabricating a stronger Al-based composite via HEBM.

1. INTRODUCTION

Aluminum matrix composites (AMC's) have become the material of choice in lightweight high strength applications. AMCs have a relatively ductile matrix and a harder dispersed phase, e.g. SiC_p, Al_2O_3, TiC, etc. In addition, mo AMCs can also be fabricated via low cost processing /1/ and bear unique thermal properties and wear resistance with potential applications in aerospace structure and components /2, 3/. Nonetheless, a common problem in AMCs is the difficulty in creating a strong matrix/reinforcement interface while avoiding detrimental chemical reactions between particles matrix /4/ or sensitizing the interface to corrosion /5/. One solution is the use of a dispersed phase, which is: a) thermodynamically stable with the matrix, and b) a nucleation agent for the Al matrix to ensure appropriate matrix/dispersoid load transfer achieved via good cohesion between both phases. Such material is a precipitation-hardenable Al/AlB_2 composite developed in recent years /6/. However, the addition of other metal diborides as potential reinforcing particles (highly desirable due to their high hardness) remains an issue for this AMC.

The present work aimed at manufacturing an aluminum matrix composite reinforced with hard MgB_2-based particles as an alternative lightweight material for aerospace applications. However, proper incorporation of MgB_2-based dispersoids is hampered by the lack of enough wettability between that diboride and liquid aluminum upon processing. Seemingly liquid Al high surface tension and oxide layer formation on the diboride hinder particle/matrix cohesiveness. The oxide layer formed on liquid aluminum upon processing may also prevent incorporating the particles.

* Corresponding author. E-mail: msuarez@ece.uprm.edu, Fax: 1-787-265-3816, Tel.: 1-787-832-4040 ext. 2350

At this moment, a complete Al-Mg-B phase diagram substantiated with experimental data is lacking. One example is the work by Ran and Rogl /7/, which only provides a "tentative partial isothermal section" at 900°C, limited to compositions up to 50 atomic% of each component. Two phases present in this diagram are AlB_2 and MgB_2 that, as most transition metal diborides, possess an hp3 crystal structure with space group symmetry *P6/mmm*. This is a hexagonal structure in which close-packed metal layers (Al or Mg) alternate with graphite-like (honeycomb) boron layers /8, 9/.

High energy ball milling was selected to achieve appropriate mixing and wettability between the both composite components. A number of preliminary runs were completed to study processing variables, such as rotation speed (rpm) and milling time, to determine the optimal settings that would lead to the desired mechanical mixing. Those preliminary tests also revealed that the mechanically alloyed system, i.e. Al + metal diboride, is of ductile-brittle nature, the ductile component being aluminum and the brittle one, the diboride powder.

2. EXPERIMENTAL PROCEDURE

A vario-planetary high energy ball milling unit was used for mechanical alloying the composite components. The unit, a Fristch vario-planetary mill model PULVERISETTE 4, allowed for configuration of the speeds for grinding bowls and the support disc completely independently of each other. This makes it possible to perform both mechanical activation as well as mechanical alloying with a single mill through modification of the gear ratio. The mill was programmable (via an RS232 interface) and allowed configuring the speeds of its two grinding bowls (jars) and the support disc completely independently of each other.

Initial experiments with aluminum (with 99.9% purity) as chunks, pellets and powder (~40μm average size) mixed with MgB_2 powder (with ~44μm average size), allowed determining the optimum contact/mixing conditions for the milling process. It was observed that large aluminum chunks inhibited proper motion of the milling balls that hindered good interaction between the components. The aluminum powder caused excessive cold welding in the milling jar inner walls and balls. The best performance, i.e. less cold welding occurrence and wettability was obtained using the Al pellets. While these pellets were flattened by the ball collisions, the magnesium diboride particles fragmented and became mostly embedded into the ductile aluminum. Further optimization of the ball milling parameters led to improved mixing between components and a substantial reduction of cold welding.

Figure 1 is a simplified version of the Al-Mg-B equilibrium phase diagram, as published by Ran and Rogl /7/ extended to 100% of each component. The diagram displays the composite compositions selected to be fabricated for this research.

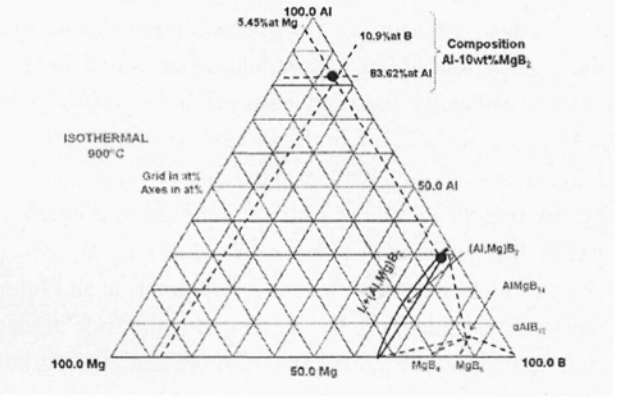

Fig. 1: Extended ternary phase diagram Al-Mg-B up to 100% at isothermal 900°C based on MSIT ternary diagram [4]

As aforementioned, 99.9% pure aluminum pellets (size range 800μm-2500μm) and MgB_2 powder (~44μm) were selected to formulate two mixtures: Al-5wt%MgB_2 and Al-10wt%MgB_2. The mixtures would undergo 8 hours of milling time with nineteen WC balls (10mm diameter), using a -2 impact parameter and 1000 rpm. Figure 2 shows a poor mixing after ballmilling using non-optimal parameters (a) and an appropriate mixing between components using the optimal parameters (b).

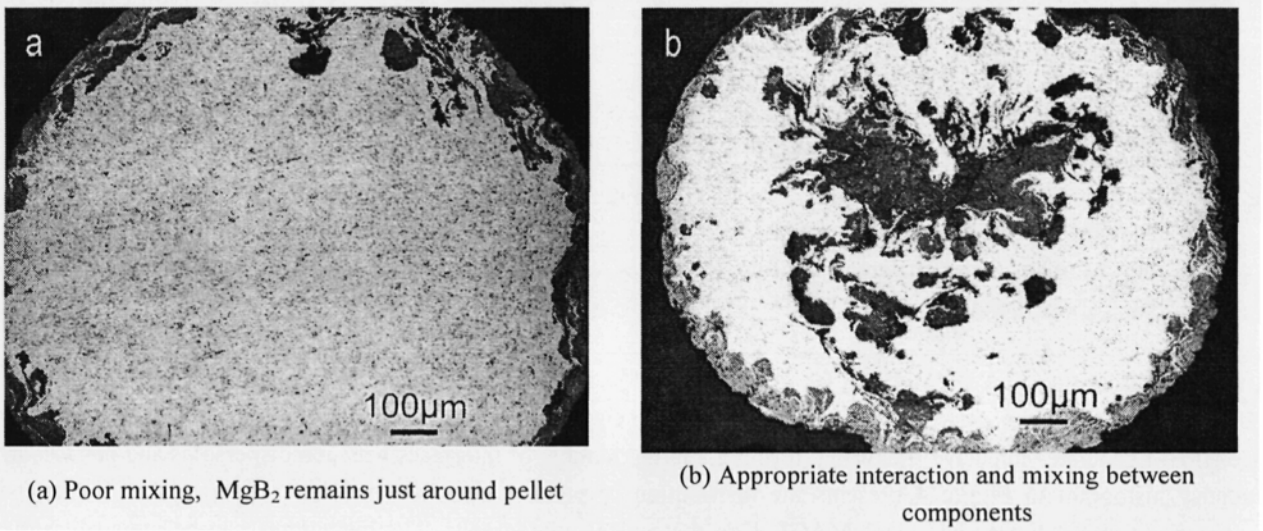

(a) Poor mixing, MgB_2 remains just around pellet

(b) Appropriate interaction and mixing between components

Fig. 2: Al pellets with MgB_2 at 50X after ballmilling

The mechanical alloyed specimens were then compacted into coin-shaped samples. These samples were then encapsulated in an evacuated quartz tube and treated in an electrical furnace at 900°C for one hour to further improve the intimate contact between diboride and aluminum.

All samples were ground and then polished using a 0.05μm SiO_2 emulsion. An ultrasonic cleaner helped eliminate cross contamination in the samples. An inverted optical microscope was used in metallographic analysis. Particle size and volume fraction of phases were measured using Image J public domain software /10/. Complementary studies included x-ray diffraction (XRD), scanning electron microscopy (SEM) and differential thermal analysis (DTA), as explained in a later section.

3. RESULTS

Image analysis of optical micrographs of the composites indicated a noticeable size distribution of the diboride particles starting from large ones (<23μm) and including submicron ones. The resulting microstructures are presented in Figures 3a and 3b. Figure 3a shows the reinforcing particles (large and submicron) embedded in the aluminum matrix for the Al-10wt%MgB_2 composite. Figure 3a displays the β + Al eutectic and diborides to demonstrate the morphological difference between β and diboride phases. Chemical composition of both phases was determined by energy dispersive spectroscopy (EDS), as explained below.

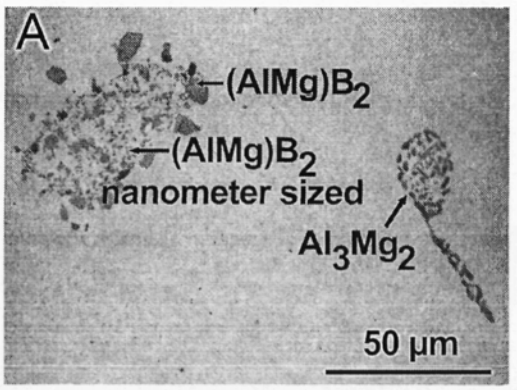

Fig. 3(a): Microstructure Al-10wt% MgB_2 composite showing corresponding phases embedded in the Al matrix and different reinforcement sizes (B, nB) and the eutectic (E)

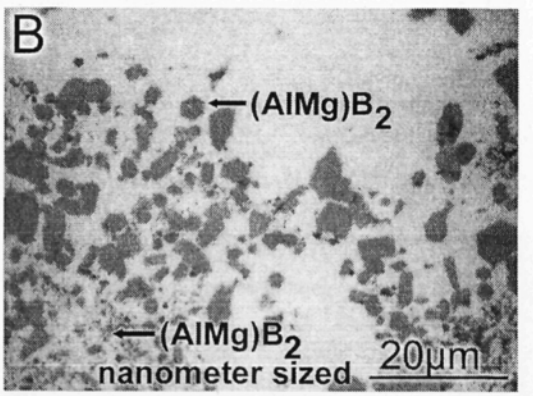

Fig. 3(b): Micrograph of Al-10wt% MgB_2 composite showing both reinforcements sizes (B) larger particles and (nB) loci of submicron particles cluster.

In both composites, i.e. Al-5wt%MgB_2, Al-10wt%MgB_2, the reinforcement particles found differed in size and quantity requiring a more rigorous statistical analysis. The size distribution of the diboride particles was predictable since HEBM generates intensive fracturing, forming a larger number of interfaces between dispersoids and matrix. The frequency histogram in Figure 4 presents the distribution of particle sizes above 0.2µm (limitation of the optical microscope used), as measured using IMAGE J on the optical micrographs. The histograms can be modeled with a lognormal distribution with 3.6µm mean particle size for samples containing 10wt%MgB_2 and 7.33µm mean particle size for samples with 5wt%MgB_2 (Figure 4).

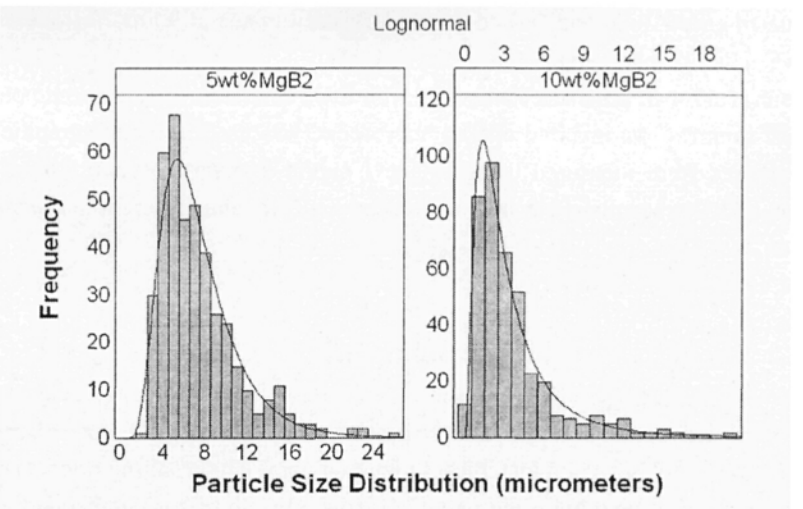

Fig. 4:.Frequency histogram of particle size distribution for each composite

To quantify the volume fraction of the reinforcing particles, micrographs at 200x and 500x magnification were analyzed with Image J. The average volume fraction in the composite with 10wt%MgB_2 was 23.73%, while for the 5wt%MgB_2 composite the mean volume fraction was 22.44%.

Vickers microhardness (HV) was measured on the matrix of both composites. The highest matrix hardness was found in samples containing 5wt%MgB_2 (Figure 5). The mean microhardness for the 10wt%MgB_2 composite was 32.65 HV while for 5wt%MgB_2 one, 43.53HV.

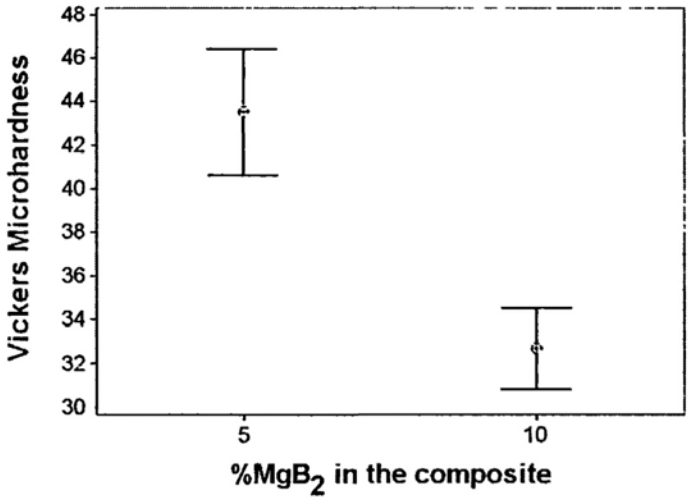

Fig. 5: Vickers microhardness in the matrix for 5wt%MgB_2 and 10wt% MgB_2 composites

These results required a more careful study of the composites using a high resolution scanning electron microscope (SEM). Working at its detection limit the instrument revealed qualitatively larger amounts of submicron and nanosized reinforcement particles were present in the 5wt%MgB_2 composite in addition to micronsized borides. The smaller particles were not visible in the optical micrographs used for image analysis but have a direct influence in the matrix microhardness, as explained below. In summary, the ball milling processing created two types of fractured particles (i.e. bimodal size distribution): ones that are very small (slightly visible in Figure 5) and larger ones (micronsized) whose effect is analyzed in the following paragraphs.

Microhardness was measured using a Vickers indenter in areas containing both reinforcing particles and Al matrix. The corresponding volume fractions of each phase had been previously quantified for that area via Image J. The microhardness values recorded varied as a function of the particle volume percent, which ranged from 12.6% to 28.1%. Figure 6 shows three optical micrographs where the microindentations are apparent. The fitting equation for the experimental data was obtained by linear regression analysis and is presented in equation (1):

$$\text{Microhardness (GPa)} = 38.65 \cdot e^{(0.03899 \cdot \text{Vol.Fraction})} \quad (1)$$

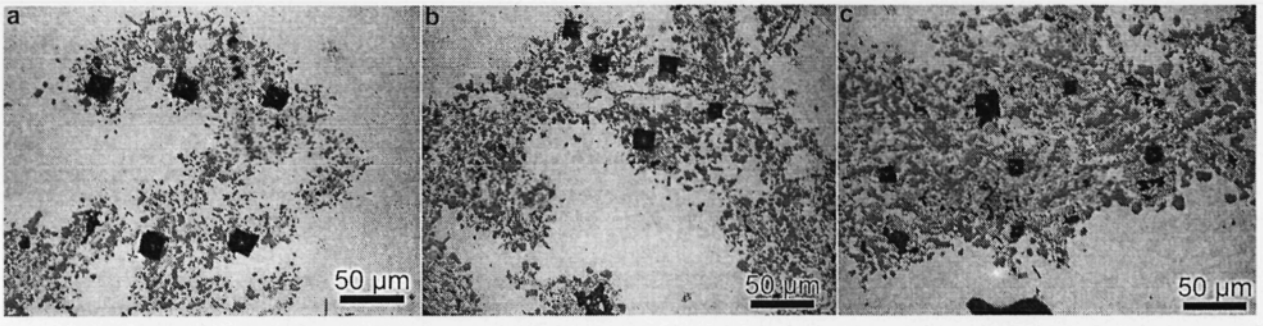

(a) Vol.fract 22.8%, 86.4 HV, Al-5wt%MgB_2 (b) Vol.fract 17%, 57.1 HV, Al-5wt%MgB2 (c) Vol.fract 27.9%, 97.18 HV, Al-10wt%MgB2

Fig. 6: Vickers microhardness indentations over reinforcement areas

Equation 1 can be used to extrapolate the expected microhardness value for pure $(AlMg)B_2$, i.e. , a diboride volume fraction equal to 1, i.e. 100% in volume percent. Figure 7 shows the experimental data points obtained from both composites and the fitted model (continuous line). Table 1 presents the measured (experimental) values of microhardness in GPa, the fitted microhardness values (according to equation 1), the computed squared residuals (following a linear regression analysis) and the resulting coefficient of determination R^2 of the regression model, which is very high. It should be noted that in these composites HEBM processing method could not achieve higher loadings (volume percent) of reinforcements than 28.1%. As a consequence of such experimental limitation, there is a large gap between about 28.1% and 100% in Figure 7.

Table 1

Measured microindentation values and resulting linear regression fitted values according to equation (1).

Volume Percent of Diborides	Measured Microhardness (GPa)	Fitted Microhardness (GPa)	Squared Residuals
0	0.3788	0.3790	$7.31973 \cdot 10^{-8}$
12.1	0.6166	0.6159	$4.73836 \cdot 10^{-7}$
12.6	1.0378	0.6284	$1.67618 \cdot 10^{-1}$
12.9	0.6801	0.6360	$1.94494 \cdot 10^{-3}$
17	0.5596	0.7497	$3.61622 \cdot 10^{-2}$
17.9	0.8908	0.7773	$1.28840 \cdot 10^{-2}$
18.1	0.8381	0.7836	$2.97256 \cdot 10^{-3}$
19.3	0.8847	0.8222	$3.90864 \cdot 10^{-3}$
19.8	0.8149	0.8389	$5.76788 \cdot 10^{-4}$
20.9	0.9261	0.8767	$2.43641 \cdot 10^{-3}$
22.8	0.9524	0.9462	$3.81132 \cdot 10^{-5}$
23.5	1.3519	0.9731	$1.43465 \cdot 10^{-1}$
24.3	0.7021	1.0049	$9.16955 \cdot 10^{-2}$
25.5	0.6907	1.0545	$1.32312 \cdot 10^{-1}$
27.9	0.8467	1.1610	$9.87962 \cdot 10^{-2}$
28.1	0.7611	1.1704	$1.67547 \cdot 10^{-1}$
100	**18.8600**	**20.9507**	**4.37097**
		Total	6.8203
		R^2	0.9830

In order to corroborate the adequacy of the equation (1) a nano indentation (4000μN of max load) was conducted on a large diboride particle (~4μm). The measured hardness value was 18.86 GPa, which is very close to the hardness predicted by Equation (1). This number is highlighted in Table 1. The inset on Figure 7 shows an image of the nanoindentation obtained in a high resolution scanning electron microscope.

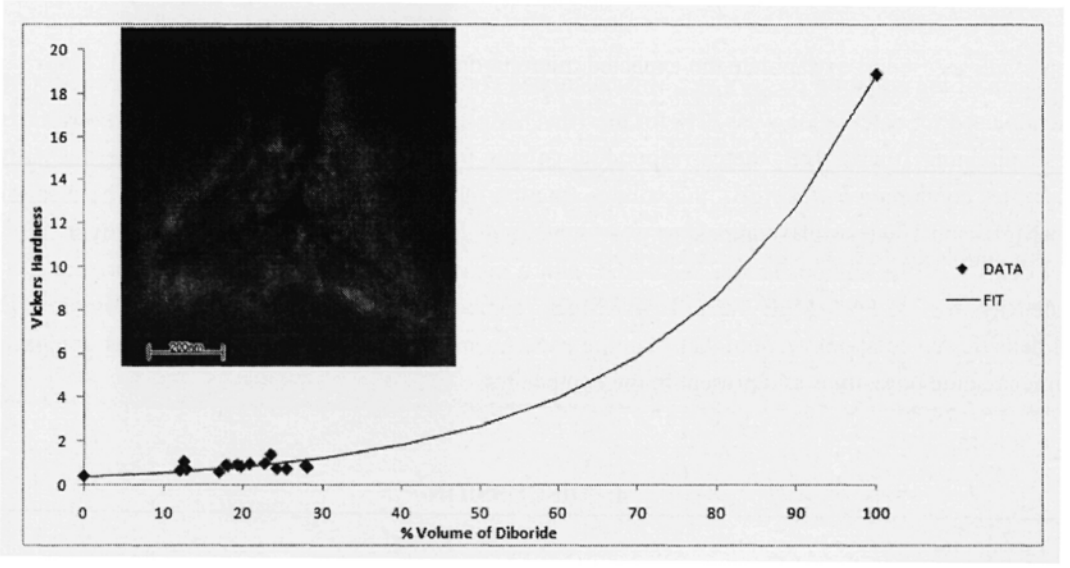

Fig. 7: Vickers Hardness vs % Volume of diboride, with experimental data fit.

Figure 8 presents a plot using the combined microindentation data measured in both compositions (5wt% and 10wt%MgB_2) versus average particle size around the indented area. The result shows that higher values of microindentation (measured in Vickers numbers, i.e. HV or kgf/mm^2) were found for indented areas with the smallest (measureable) particle sizes. The line corresponds to Equation (2), which was fitted by linear regression (least-squared method).

$$\text{Microindentation (kgf/mm}^2\text{ or HV)} = 290.34 \cdot (\text{Part.Size})^{-0.7} \quad (2)$$

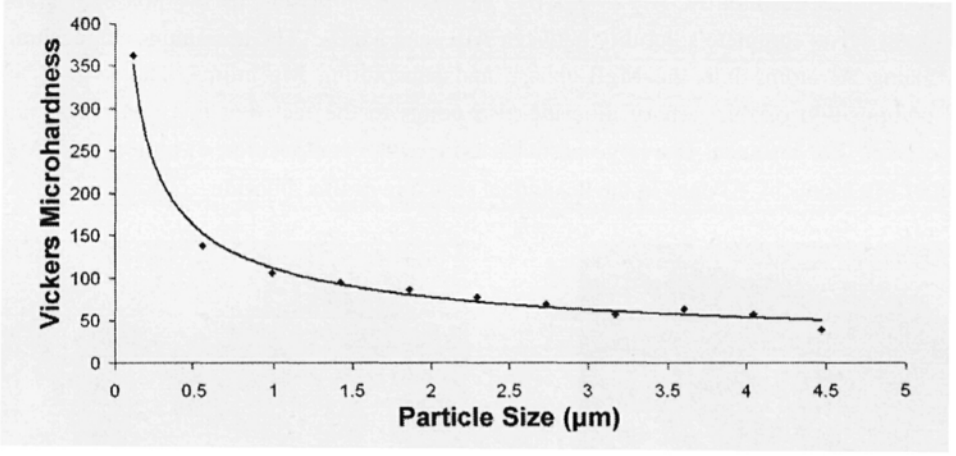

Fig. 8: HV vs. Particle size using data of both compositions

Composite densities were calculated by theoretical and practical means. First, theoretical density for both compositions was calculated using the rule of mixtures according to equation (3) where ρ is density and V, the component (reinforcement or matrix) volume fraction.

$$\rho_{Theoretical} = \rho_{matrix} \cdot V_{matrix} + \rho_{reinforcement} \cdot V_{reinforcement} \quad (3)$$

The first term of the equation $\rho_{matrix} \cdot V_{matrix}$ was calculated considering both Al matrix and eutectic β (Al_3Mg_2). The volume fraction used for calculation was: 22% for the 10wt%MgB_2 composite and 20% for the 5wt%MgB_2 one.
For samples containing 10wt%MgB_2 the corresponding volume fraction of Al_3Mg_2 measured experimentally was 15%, while for samples containing 5wt%MgB_2, the volume fraction of this eutectic phase was 11%. The theoretical density for Al-5wt%MgB_2 and 10wt%MgB_2 composites was found to be 2.70 g/cm^3 and 2.68 g/cm^3 respectively.

Practical density of the composite was measured with a picnometer using the Archimedes principle. The average measured density for Al-5wt%MgB_2 and 10wt%MgB_2 composites was 2.57g/cm^3 and 2.54g/cm^3, respectively. Theoretical densities calculations were higher than the experimental one, indicating that even after compaction and the 900°C treatment, some porosity is still present in the composites.

4. DISCUSSION

From the measured particle sizes it is apparent that the diboride reinforcing particles (originally with an average size of 44 μm) have fractured and, likely, refractured many times to generate the micron-sized, and submicron dispersoids. An interesting feature of the post-ball milled composites is that the diboride particles cleaved along specific planes, likely the $\{1\,\bar{1}\,00\}$ to produce hexagonal shapes. Figures 9a and 9b present two SEM images were the morphology of the cleaved reinforcements can be appreciated; the different shapes are due to different spatial orientations: the hexagonal one having its c axis perpendicular to the image. Energy dispersive spectroscopy (EDS) standardless analysis on both types of particles produced similar results. Figure 10 presents a representative EDS spectrum obtained from a reinforcement particle. As it can be observed, Al, Mg, and B are present in this 200 nm particle. After ZAF correction, the average chemical composition measured in several particles was Al 10 ± 5 at.%, Mg 24 ± 6 at.% and B 66 ± 2 at/%. This consequential finding indicates that the diboride particles are no longer MgB_2 after processing but a ternary phase with an approximate chemical formula of $Al_{0.29}Mg_{0.71}B_2$. This is not surprising as the phase diagram in Figure 1 indicates that there likely exists complete solubility between AlB_2 and MgB_2. The aluminum magnesium diboride was then formed by diffusing Al atoms into the MgB_2 phase and substituting Mg atoms. The large dispersion of the measured chemical composition of this ternary diboride also points to the fact that this phase was not equilibrated throughout the processing. For instance, few large particles evinced the composition of almost pure MgB_2 indicating minimal substitution of Mg atoms by Al ones in the hexagonal structure of this diboride.

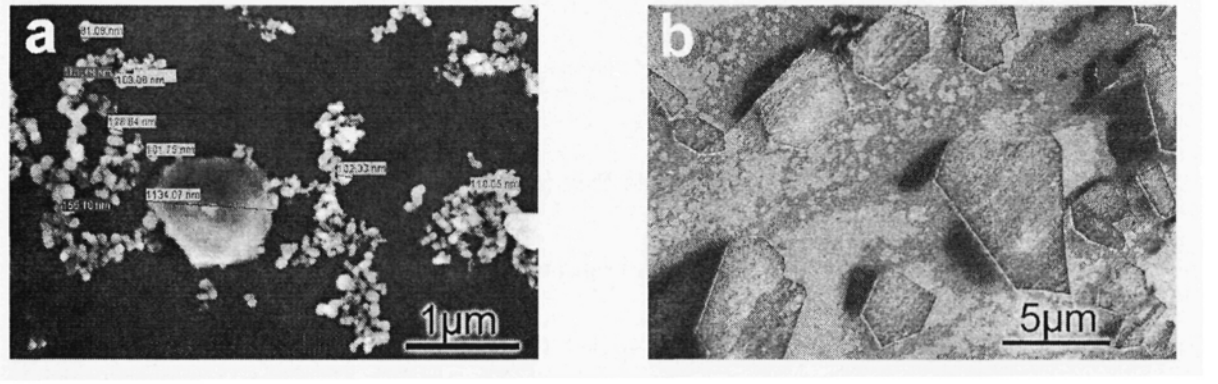

(a) Morphology of particles (b) Dissimilar sizes of (AlMg)B_2 particles

Fig. 9: SEM images

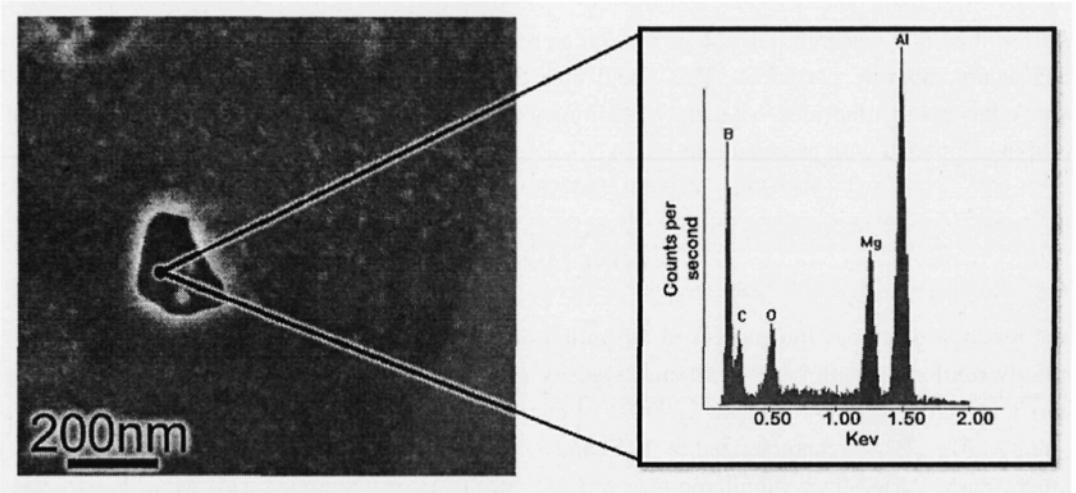

(a) Particle at 200nm (b) Corresponding EDS of the particle

Fig. 10: SEM image of (AlMg)B2 reinforcement

For the aforementioned reasons, it was necessary to corroborate the nature of all phases present in the composites, as those observed in Figures 3a and 3b. To this purpose the same specimens imaged in both figures were used for phase identification. This was done using an x-ray diffractometer (Cu Kα radiation) operated at 40mA and 40kV with steps of $2\theta = 0.02°$ and 2 seconds at each step. The diffraction patterns were analyzed using the Match!® v. 1.9 package, which is a user-friendly software for phase identification from x-ray powder diffraction data and was developed by *Crystal Impact* (www.crystalimpact.com). To this purpose Match! was furbished with a PDF2 powder diffraction database.
The diffractogram in Figure 11 corroborates the presence of all phases observed in Figure 3a and 3b. However there is one evident MgB_2 peak, which indicates that not all MgB_2 particles have substitutionally dissolved Al atoms. There are small peaks between 30° to 50° that appeared around $AlB_2(101)$, Al(100)(111)(200), and $MgB_2(101)$ peaks and are associated with the ternary $(AlMg)B_2$ phase.

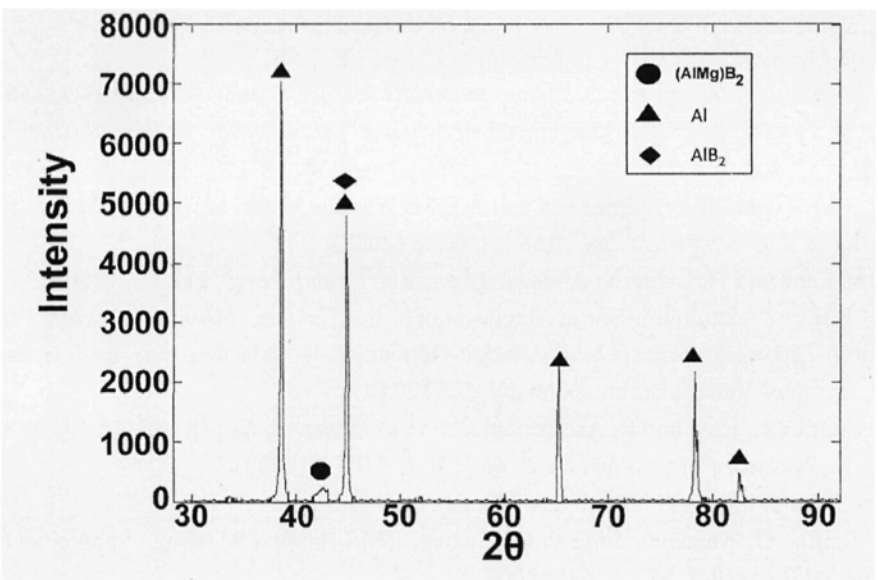

Fig. 11: XRD pattern for $(AlMg)B_2$ composite. Al , MgB_2, AlB_2

As the end result of this research, HBEM proved be an adequate alternative to fabricate an AMC reinforced with aluminum magnesium diboride particles. This could open the door to prepare other aluminum-based composites reinforced with other metal diborides. Recently, additional experiments with the same procedure applied to other systems have been completed with promising results /11/.

CONCLUSIONS

The present research discusses the successful utilization of high energy ball milling to fabricate a new Al matrix composite initially reinforced with MgB_2 particles. Density measurement indicated the occurrence of some porosity during the fabrication process. The treatment at 900°C of the ball milled composites caused the MgB_2 dispersed phase to transform into $Al_xMg_{1-x}B_2$, as characterized by EDS and x-ray diffraction. The resulting particles sizes, as observed with optical microscopy, varied from submicron ones to large ones (<23μm). Submicron $Al_xMg_{1-x}B_2$ particles (detected only via high resolution SEM) likely caused high microhardness values when the composite matrix was indented. A regression model permitted relating the volume fraction of particles with the resulting hardness. From a mechanical designer's viewpoint this fact would be helpful upon selecting the particle loading needed to achieve a specific strength.

ACKNOWLEDGMENTS

The authors would like to kindly acknowledge Michael Ramirez and Gabriel Cruz from the Hewlett Packard SEM Laboratory in Aguadilla, Puerto Rico, for their help with the SEM/EDS analysis. This research is based upon work supported by the National Science Foundation under Grants N° DMR-0351449 (PREM Program) and HRD-0833112 (CREST Program).

REFERENCES

1. O.M. Suárez, *J. of the Mechanical Behavior of Materials*, **12** [4], 225 (2001).
2. Q. Ouyang, R. Li, W. Wang, G. Zhang and D. Zhang, *Materials Science Forum*, **546-549**, pt.3, 1551 (2007).
3. Z.H. Melgarejo, O.M. Suárez and K. Sridharan, *Composites A: Applied Sci. & Manufacturing*, **39** [7], 1150 (2008):.
4. S.W. Ip, R. Sridhar, J.M. Toguri, T.F. Stephenson and A.E.M. Warner, Mater. Sci. Eng. **A244**, 31 (1998).
5. H. Ding and L.H. Hihara, *J. Electrochem. Soc.*, **155** [5], C226 (2008).
6. O.M. Suárez, J. Yupa Luna and H. Calderón Arteaga, *Trans. Am. Foundry Soc.*, **111** 159 (2003).
7. Q. Ran and P. Rogl, "Aluminium-Boron-Magnesium," in *Ternary Alloy Systems, Phase Diagrams, Crystallographic and Thermodynamics Data*, Landolt-Börnstein. W. Martienssen, Ed., Group IV: Physical Chemistry, Vol. 11, Springer Verlag, Berlin, Germany, 52 (2004).
8. P. Vajeeston, P. Ravindran, C. Ravi and R. Asokamani, *Physical Review B*, **63** [4], 045115-1 (2001).
9. I. Loa, K. Kunc and K. Syassen, *Physical Review B*, **66** [13], 134101-1 (2002).
10. National Institutes of Health, http://rsb.info.nih.gov/ij/index.html [online].
11. H.E. Calderón, C. Smith, O. Menéndez and O.M. Suárez, TMS Annual Meeting, Supplemental Proceedings: Materials Processing and Properties, Vol. 3, 425 (2008).